

Article

Co-immobilization of an Enzyme System on a Metal-Organic Framework to Produce a More Effective Biocatalyst

Raneem Ahmad , Jordan Shanahan, Sydnierizaldo, Daniel S. Kissel *  and Kari L. Stone * 

Department of Chemistry, Lewis University, Romeoville, IL 60446, USA; raneemahmad@lewisu.edu (R.A.); jordanjshanahan@lewisu.edu (J.S.); sydnierizaldo@lewisu.edu (S.R.)

* Correspondence: kisselda@lewisu.edu (D.S.K.); kstone1@lewisu.edu (K.L.S.); Tel.: +1-815-588-7435 (D.S.K.); +1-815-834-6109 (K.L.S.)

Received: 28 March 2020; Accepted: 30 April 2020; Published: 2 May 2020



Abstract: In many respects, enzymes offer advantages over traditional chemical processes due to their decreased energy requirements for function and inherent greener processing. However, significant barriers exist for the utilization of enzymes in industrial processes due to their limited stabilities and inability to operate over larger temperature and pH ranges. Immobilization of enzymes onto solid supports has gained attention as an alternative to traditional chemical processes due to enhanced enzymatic performance and stability. This study demonstrates the co-immobilization of glucose oxidase (GO_x) and horseradish peroxidase (HRP) as an enzyme system on Metal-Organic Frameworks (MOFs), UiO-66 and UiO-66-NH₂, that produces a more effective biocatalyst as shown by the oxidation of pyrogallol. The two MOFs utilized as solid supports for immobilization were chosen to investigate how modifications of the MOF linker affect stability at the enzyme/MOF interface and subsequent activity of the enzyme system. The enzymes work in concert with activation of HRP through the addition of glucose as a substrate for GO_x . Enzyme immobilization and leaching studies showed HRP/ GO_x @UiO-66-NH₂ immobilized 6% more than HRP/ GO_x @UiO-66, and leached only 36% of the immobilized enzymes over three days in the solution. The enzyme/MOF composites also showed increased enzyme activity in comparison with the free enzyme system: the composite HRP/ GO_x @UiO-66-NH₂ displayed 189 U/mg activity and HRP/ GO_x @UiO-66 showed 143 U/mg while the free enzyme showed 100 U/mg enzyme activity. This increase in stability and activity is due to the amine group of the MOF linker in HRP/ GO_x @UiO-66-NH₂ enhancing electrostatic interactions at the enzyme/MOF interface, thereby producing the most stable biocatalyst material in solution. The HRP/ GO_x @UiO-66-NH₂ also showed long-term stability in the solid state for over a month at room temperature.

Keywords: enzyme co-immobilization; metal-organic framework; biocatalysis

1. Introduction

Due to current advances in biotechnology, the commercial value of enzymes as biocatalysts has increased dramatically in recent years [1–4]. The use of biocatalysts for industrial applications is attractive because of the benefits offered by enzyme proteins, including high selectivities, diverse functionalities, and the promotion of greener chemistries [4]. However, the fragile nature of enzymes and narrow operating temperatures and pH ranges have hampered their use commercially. One strategy of preparing enzymes that are more robust to withstand pH, temperature, and/or organic solvents is by immobilizing enzymes on solid supports. In this way, enzymes may be altered that may increase their activity, specificity, or selectivity of the target reaction [5]. Industrially, there is a great deal of

interest in the immobilization of enzymes onto solid supports, where an enzyme is attached to a physical surface or material by covalent and/or noncovalent interactions, which has been shown to enhance enzyme stabilities and activities [1,4,6,7]. Solid supports also offer potential for enzyme recovery and recyclability, which increases their commercial value [1,4,6,8–12]. Many reports investigating enzyme immobilization have shown utility for applications in organic syntheses, such as warfarin catalysis and even esterification reactions where immobilization was crucial for long term use [7,13–17]. Several of these immobilization studies explore techniques and methodologies surrounding enzymes immobilized on relatively new materials, such as Metal-Organic Frameworks (MOFs) [1]. These materials have proven to be capable of many different types of immobilizations, both noncovalent and covalent by nature, including surface attachment, cross linkage, covalent linkage and bonding, and encapsulation [16,18–24].

Metal-organic frameworks are coordination networks composed of organic linkers and inorganic nodes containing potential void space with large surface areas [1,25–29]. MOFs stand out as effective solid supports for immobilization due to their highly tunable organic linkers and potential void space, which are ideal for the design of strong guest–host interactions. The target MOFs, UiO-66 and UiO-66-NH₂ used in this study as solid supports for enzyme co-immobilization of HRP and GO_x, create new biocatalytic materials referred to as HRP/GO_x@UiO-66 and HRP/GO_x@UiO-66-NH₂. The Zr-based UiO MOFs were chosen for immobilization because of their high thermochemical stability, making them amongst the most stable MOFs known, as well as their high degree of tunability [30]. Encapsulation or diffusion into potential void space is typically the focus of enzyme immobilization studies. This requires the use of MOFs with large organic linkers that can be difficult to synthesize or expensive to purchase, and typically have much lower stabilities in solution. The highly tunable surface chemistry of MOFs, however, remains an under-utilized avenue for enzyme immobilization despite the simplicity in pre- and post-synthetic modifications that can enhance interactions at the enzyme/MOF interface. This is especially true for co-enzyme systems where surface immobilization has less probability of hindering enzyme activity. The UiO-66-NH₂ MOF, in particular, features an amine group off the organic linker that could serve as a site for covalent bond formation or increased hydrogen-bonding at the enzyme/MOF interface. Increasing the interfacial stability of the enzyme/MOF biocatalyst is expected to increase immobilization loading, thereby improving stability and catalytic activity.

Co-immobilization of enzymes on solid supports have been studied for various applications with multiple systems in the past decade [5,6,9–12,30–33]. Immobilization of two or more enzymes has its advantages and disadvantages. For systems that involve cascade reactions, co-immobilization offers a kinetic advantage where the first product is in close proximity to the second enzyme that is activated by the first product. This removes the potential lag time of the diffusion of substrate at high concentrations for the second enzyme, which allows the second enzyme to be activated at high concentrations from the first product [31]. Enzyme co-immobilizations have shown to be useful for two main tasks in catalysis: (1) to act as a pathway for intermediate reaction products to proceed directly to a second enzyme, and (2) to maximize intermediate and avoid the loss of intermediate due to diffusion or instability [12]. Co-immobilizing prevents high concentrations of intermediates or reaction products to inhibit the enzymes by restricting local concentration as discussed in the review by Betancor et al. on co-immobilized coupled enzymes [12]. While individual immobilization offers some of these advantages, the strategy of co-immobilization can have even more positive effects, such as fast conversion of substrate to product, easy separation of enzyme and product, and higher efficiency [9]. Furthermore, co-immobilized or multienzyme systems have shown better performance than single enzyme systems due to restriction in the diffusion of unstable intermediates [9]. Garcia-Galen et al. reviewed how immobilization strategies affect and many times improve enzyme performance. They describe how co-immobilization also presents some challenges: (1) immobilization of all enzymes must use the same immobilization strategy, and (2) the robustness of the overall biocatalyst will be determined by the least stable enzyme [31,34]. When co-immobilizing enzymes, there must be considerations of whether separate immobilization of individual enzymes or co-immobilization on the same solid support utilizing the same reaction conditions [31]. By using the

same immobilization protocol for a multienzyme system, the researcher is assuming that immobilization of each will be similar, which may result in the loss of immobilization advantages, if this is not the case. A proposed strategy to avoid this problem is to co-immobilize the most stable enzymes, which was shown in a study done by Rios et al. [35]. The study showed that when lipase with different stabilities were co-immobilized, the most stable lipase dominated co-immobilization [35]. A benefit of our system in this study is that the surface of the MOF is tunable as we report differences in stabilities due to changes in MOF linker functionalities. The UiO-66 MOFs, in particular, can readily be functionalized post-synthetically to alter surface properties, as demonstrated by Marshall et al., which could allow for the immobilization of different individual enzymes [36]. Other disadvantages of co-immobilization or multienzyme systems are the randomness of the enzyme concentrations, the inability to use large multidomain enzymes, and the supports can be a diffusion barrier [9,12]. In an attempt to improve co-immobilization and multienzyme systems, a rational design has been recently developed by quantitative tools using yeast cell surface to study how multienzyme assemblies form, molecular crowding, and how to maximize enzyme density [37,38]. For co-immobilization of enzymes to work properly, both enzymes need to be immobilized on the solid support. This study demonstrates that our MOF system is suitable for enzyme co-immobilization.

The results presented herein focus on co-immobilization of two enzymes onto the surface of zirconium-based MOFs using a facile adsorption technique to create novel biocatalysts held together by strong, noncovalent interactions at the enzyme/MOF interface. The enzyme system in this investigation consists of glucose oxidase (GO_x) from *Aspergillus niger* and horseradish peroxidase (HRP). Glucose oxidase is available commercially and is used for a wide range of applications in chemical industries related to biosensors, biofuel cells, food and beverage production, and textile manufacturing [7,39]. Horseradish peroxidase is a common enzyme used for organic syntheses that is often coupled with other enzymes for immunoassays, chemiluminescent assays, and water treatment assays [40,41]. These two enzymes are known to work cooperatively in systems where sugar is oxidized by GO_x to produce hydrogen peroxide, which activates the HRP enzyme that in turn oxidizes an organic substrate [41,42].

In relation to this paper, the co-immobilization of glucose oxidase (GO_x) and horseradish peroxidase (HRP) generates hydrogen peroxide in situ by the oxidation of glucose from GO_x to activate HRP. The two enzymes have been co-immobilized in previous studies for applications such as catalysis in organic syntheses and biosensing [9,38,43–52]. Coordination polymer formation was previously utilized by Jia and colleagues to co-immobilize HRP/ GO_x by binding a nucleotide and a metal, guanine and copper, for a biocompatible composite in glucose biosensing technology [46]. The two enzymes were also investigated by Zhu et al. for glucose biosensing by co-immobilization on carbon nanotube electrodes, and by Chen et al. for bisphenol A detection by co-immobilization on a copper-based MOF [24,30]. Gustafsson and colleagues have reported co-immobilization by using dendronized polymer and mesoporous silica nanoparticle layers, which showed stability for at least two weeks [44]. Furthermore, studies that attempted to spatially control the co-immobilization of HRP/ GO_x utilizing micelles and inorganic nanocrystal–protein complexes reported similar enhanced activities and stabilities [43,53]. The coupled enzymes have also been co-immobilized on DNA-directed assemblies by conjugate covalent DNA oligonucleotides to oxidize Ampex Red [54]. While immobilizations on scaffolds such as DNA have shown to allow for spatial control, this method is costly and only stable under standard conditions [38].

MOFs have proven to be a more tunable solid support for HRP/ GO_x in studies that investigate factors influencing immobilization such as changes in surface area, magnetic properties, and, in this work, linker functionalization [8,47,48]. Chen et al. showed how magnetic nanoparticles can be used in co-immobilization of HRP/ GO_x to tune layers of enzymes on the MOF HKUST-1 [48]. Synthesis studies reported by Lou et al. have immobilized soybean epoxide hydrolase (SEH) onto UiO-66-NH₂ to synthesize vicinal diols by a crosslinking technique [13]. Additionally, Wu et al. have reported a single immobilization by encapsulating a three enzyme/MOF composite to synthesize purpurogallin using the

MOF ZIF-8, HRP, cytochrome c (Cyt c), and *Candida antarctica* lipase B (CALB) [47]. This investigation, however, demonstrates that effective immobilization of the HRP/GO_x coenzyme system can be accomplished through adsorption to the MOF surface by simply incubating in a buffered solution for 24 hours at cold temperatures. While prior investigations have focused on producing novel biocatalysts using more complex techniques, this paper focuses on understanding the effect of linker functionalization on adsorption at the enzyme/MOF interface, and how it affects immobilization, stability, and activity in a bi-enzymatic system.

2. Results and Discussion

2.1. The Biocatalytic Enzyme System

A biocatalytic system was created to verify co-immobilization and test the catalytic activity of HRP/GO_x@UiO-66 and HRP/GO_x@UiO-66-NH₂ in the production of purpurogallin from pyrogallol. Purpurogallin has been shown to have inhibiting properties and anti-inflammatory effects potentially useful in the pharmaceutical industry [55–58]. Pyrogallol is known for its auto-oxidation properties, and is often used to synthesize purpurogallin using a catalyst [59]. Purpurogallin has been synthesized from pyrogallol using reconstituted forms of HRP containing synthetic hemes in the presence of H₂O₂ [60]. This biocatalytic system, however, utilizes the oxidation of glucose to catalyze the oxidation of pyrogallol to purpurogallin in the presence of HRP. Figure 1 shows the overall procedure used with the enzyme/MOF biocatalytic materials investigated. The reaction mixture initially consists of glucose, pyrogallol, and the enzyme/MOF composite (HRP/GO_x@UiO-66 or HRP/GO_x@UiO-66-NH₂). Glucose is oxidized by GO_x immobilized onto the enzyme/MOF composite to produce hydrogen peroxide. Hydrogen peroxide activates HRP in the enzyme/MOF composite, which subsequently oxidizes pyrogallol to purpurogallin. Pyrogallol is colorless in solution, but oxidation to purpurogallin creates a yellow-brown solution with a λ_{max} of 420 nm in the visible range [59]. The appearance of purpurogallin can therefore be tracked by monitoring increases in absorbance at 420 nm over time. Eventually, as it becomes insoluble, the purpurogallin will precipitate out of solution as an orange solid overnight.

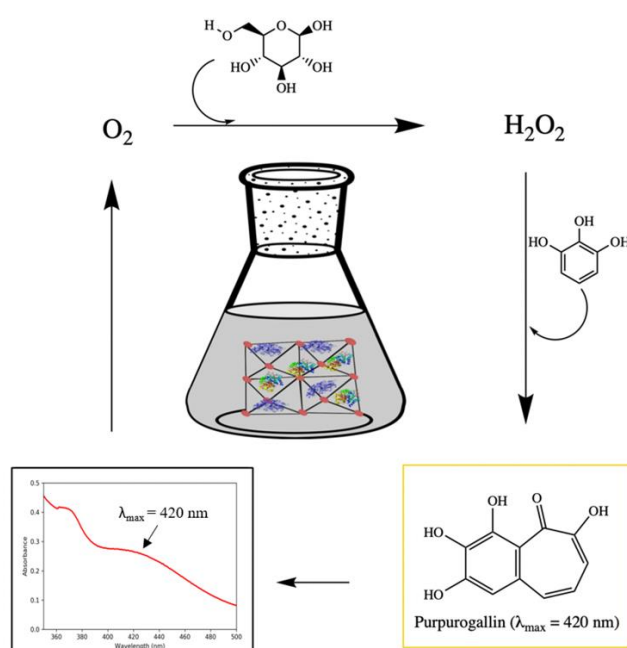


Figure 1. Biocatalytic system. Synthesis of purpurogallin from pyrogallol and glucose by catalysis using HRP/GO_x@UiO-66 or HRP/GO_x@UiO-66-NH₂. The appearance of purpurogallin is monitored spectroscopically in the visible region by tracking increases in absorbance at 420 nm.

In addition to using the biocatalytic system shown in Figure 1, protein quantification was performed using the Bradford assay to study the difference in MOF linker functionalization on enzyme immobilization and composite stability. The Bradford assay is widely used to quantify protein by binding to a dye reagent, causing a blue shift at 595 nm [61]. This assay was used to quantify the amount of enzyme immobilized onto the MOF surface from the solution during immobilization.

2.2. Zeta Potential Characterization

The MOFs used in this investigation possess uniquely dynamic surface charge characteristics with terminal carboxylic acid struts across their surfaces. These surface charges are important for enzyme loading, and can vary depending on the pH and composition of the buffered solution used during immobilization. Zeta potential measurements of solutions containing pure MOFs and enzyme/MOF composites, therefore, can indirectly probe surface charge and stability of MOF dispersions providing useful insights into differences observed in immobilization and leaching [62]. The higher zeta potentials observed in UiO-66-NH₂ (−26.67 mV) compared with UiO-66 (−18.00 mV) reflect a slightly more stable dispersion in the buffered solution utilized for immobilization. After enzyme loading, there is a sharp decrease in zeta potential observed for all enzyme/MOF composites investigated, as shown in Table 1. This is congruent with the pIs reported for HRP and GO_x, 6.35 and 4.64 respectfully, which indicate a negative charge in the pH = 7 buffered solution.

Table 1. Zeta potentials of all composite materials.

Composite	Zeta Potential (mV)
HRP/GO _x @UiO-66-NH ₂	−3.13 (s = ±8.73)
HRP@UiO-66-NH ₂	−8.46 (s = ±0.14)
GO _x @UiO-66-NH ₂	−10.00 (s = ±5.64)
UiO-66-NH ₂	−26.67 (s = ±6.68)
HRP/GO _x @UiO-66	−10.80 (s = ±4.86)
HRP@UiO-66	−7.97 (s = ±4.89)
GO _x @UiO-66	−3.38 (s = ±4.50)
UiO-66	−18.00 (s = ±5.96)

2.3. FT-IR Characterization

The FT-IR spectra of the pure MOFs UiO-66 and UiO-66-NH₂ are shown in Figure 2b. Both spectra have characteristic peaks at 1580, 1390, 723, and 670 cm^{−1} for UiO-66 and 1565, 1365, 760 and 656 cm^{−1} for UiO-66-NH₂. These peaks correspond to asymmetric O–C–O stretching, O–C–O symmetric stretching, C–C ring stretching and Zr–O stretching, respectively [63]. The spectra for UiO-66-NH₂ show additional peaks at 3317, 3444, 1416 and 1252 cm^{−1}, which correspond to the asymmetric and symmetric N–H stretching, N–H bending and the C–N stretch from the aromatic amine, respectively [64].

2.4. SEM of Enzyme/MOF Composites

SEM images of pure UiO-66 and UiO-66-NH₂ powder in Figure 3a,b show distorted octahedrons with aggregates ranging from 400 to 1000 nm in size. This is consistent with morphologies and sizes commonly reported for these MOFs [58,65,66]. Enzyme immobilization has no perceivable effects on MOF morphology in UiO-66 or UiO-66-NH₂ at 17,000× magnification. This indicates enzyme immobilization did not disrupt the MOF architectures, and that enzymes did not aggregate in appreciable quantities in the MOF suspension.

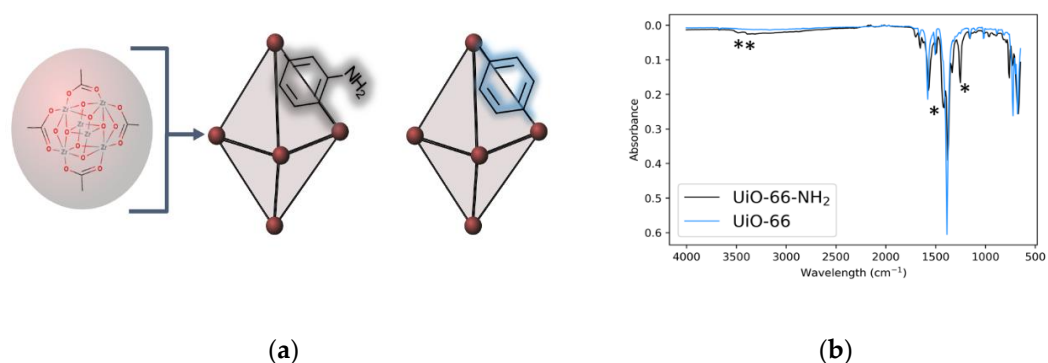


Figure 2. FT-IR spectra of UiO-66 and UiO-66-NH₂. (a) Representation of the Secondary Building Unit (SBU) of UiO MOFs with cartoons of the octahedrons showing differences in linker functionalization for UiO-66 vs. UiO-66-NH₂. (b) The FT-IR Spectra of UiO-66 and of UiO-66-NH₂. * The characterization peaks of synthesized MOF UiO-66-NH₂.

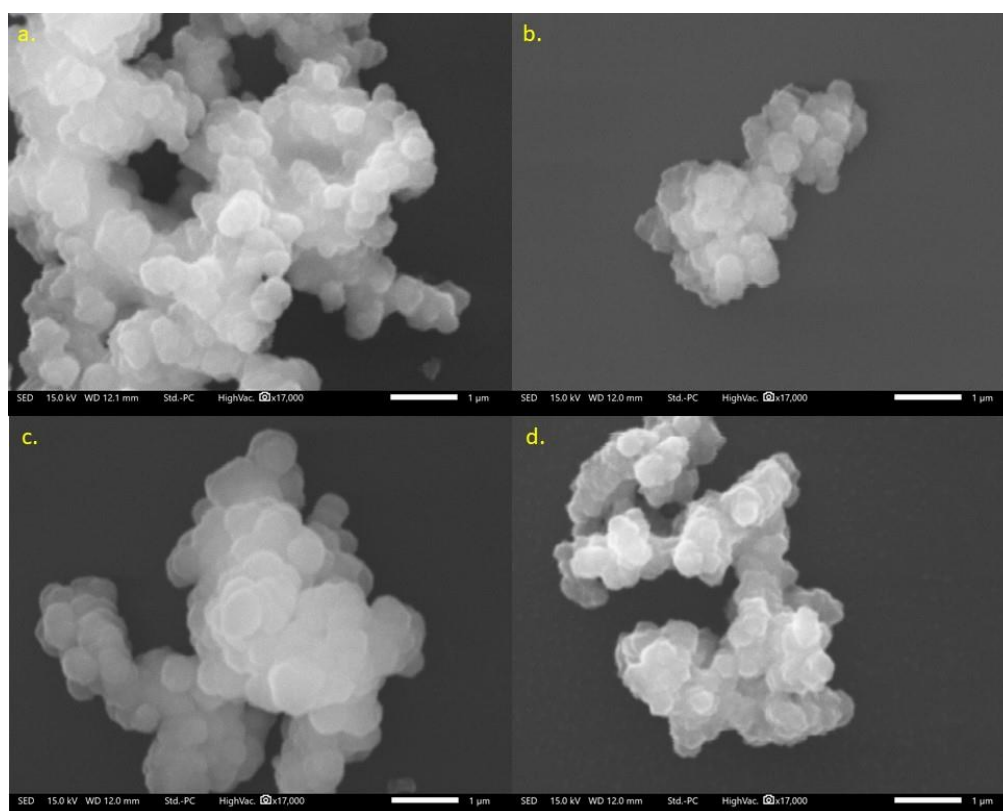
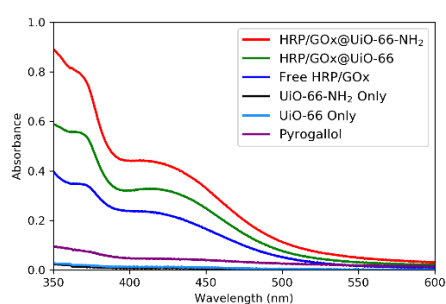


Figure 3. SEM images of MOF and enzyme/MOF composites. (a) UiO-66 aggregate cluster, (b) UiO-66-NH₂ aggregate cluster, (c) HRP/GO@UiO-66 aggregate cluster, (d) HRP/GO@UiO-66-NH₂ aggregate cluster. Both enzyme/MOF composites show clusters composed of irregular octahedrons consistent with MOF images, indicating retention of MOF morphology. All images were recorded at 17,000 \times magnification.

2.5. Purpurogallin Synthesis

Initially, enzymes were singly immobilized and tested using the formation of purpurogallin. This was done to assure that the enzyme HRP was immobilizing onto the MOF, since HRP is crucial after activation from peroxide to oxidize the organic substrate. This was also performed using GO_x to assure that the oxidation is from the enzyme HRP rather than auto-oxidation of pyrogallol. The single immobilized composites, GO_x@UiO-66-NH₂ and GO_x@UiO-66, showed little to no absorbance, which is

expected since HRP is not present to catalyze the oxidation. In the presence of hydrogen peroxide in the solution, single immobilized HRP@UiO-66-NH₂ composite did show greater absorbance values by 4% compared with the HRP@UiO-66 composite. The observation of the amino functionalized enzyme/MOF system performing better is also observed with the bi-enzymatic system. Both enzyme/MOF composites, HRP/GO_x@UiO-66-NH₂ and HRP/GO_x@UiO-66, showed enhanced catalysis of pyrogallol to purpurogallin compared with solutions containing free HRP and GO_x. The HRP/GO_x@UiO-66-NH₂ biocatalyst, which showed the greatest enzyme immobilization, produced higher absorbance values at 420 nm using the biocatalytic system, indicating greater production of purpurogallin over time. The free enzyme activity was studied by utilizing our enzyme/MOF immobilization data to replicate the enzyme concentration in the MOF to be only free enzymes in the solution for purpurogallin synthesis. Furthermore, this enzyme/MOF composite showed the greatest stability during leaching studies where each of the biocatalysts were placed in buffered solution over long periods of time. As shown in Figure 4a, the composite HRP/GO_x@UiO-66-NH₂ excels in catalyzing the synthesis of purpurogallin from pyrogallol and glucose. This is especially noteworthy considering it validates immobilization of two cooperative enzymes onto a solid support. In addition, the current data from our study indicate the parameter for expressed activity, as standardized by Lafuente et al., is increased percent enzyme activity [67]. In Table 2, the enzyme activity was calculated from the increasing absorbance of purpurogallin formation. Both composites, HRP/GO_x@UiO-66-NH₂ and HRP/GO_x@UiO-66, showed an increase in enzyme activity of 189 and 143 U/mg, respectively. The composite HRP/GO_x@UiO-66-NH₂ showed an 88.6% activity increase, while composite HRP/GO_x@UiO-66 showed only 42% activity increase compared to free enzyme HRP/GO_x displaying 100 U/mg of enzyme activity. To confirm that this observed increase in activity is indeed enzymatic and not simple auto-oxidation of pyrogallol, controls with only UiO-66-NH₂ and UiO-66 were run using the biocatalytic system, which produced almost no absorbance at 420 nm as shown in Figure 4a,b. A ¹H NMR taken of the purpurogallin product synthesized from HRP/GO_x@UiO-66-NH₂ using the biocatalytic system shown in Figure 5 verifies the presence of purpurogallin formation in the solution. This also shows the clean conversion of substrate to product using the enzyme/MOF composite as a potential biocatalyst for synthesis of organic substances.



(a)



(b)

Figure 4. Purpurogallin synthesis. (a) UV/vis absorbance values of solutions after synthesis using the biocatalytic system for all conditions investigated. The appearance of purpurogallin is tracked by monitoring absorbance at 420 nm over time, indicating HRP/GO_x@UiO-66-NH₂ is the most catalytically robust system. (b) Images of synthesized purpurogallin in the solution using the biocatalytic system for all conditions investigated. The appearance of a yellow-brown color indicates the presence of purpurogallin in the solution.

Table 2. Percent immobilization and leaching of all composite materials.

Composite	% Immobilization ^a	% Leached from Composite ^b	Enzyme Activity (U/mg) ^d
HRP/GO _x @UiO-66-NH ₂	9.91 (s = ±0.033)	35.6 (s = ±0.025)	189
HRP/GO _x @UiO-66	3.91 (s = ±0.007)	100 (s = ±0.045)	143
HRP/GO _x	0	6 ^c	100
UiO-66-NH ₂	0	0	0
UiO-66	0	0	0

^a Percent immobilization was calculated as mass percent of enzyme immobilized from solution relative to the mass of MOF present in the solution. ^b Percent leached was calculated as mass percent of enzyme leached from the composite relative to the amount of enzyme immobilized onto the MOF. ^c Free enzyme leaching was measured as the amount of enzyme that “disappears” presumably from structural denaturation. ^d Calculated from absorbance data in activity units (U per mg) of contained enzymes.

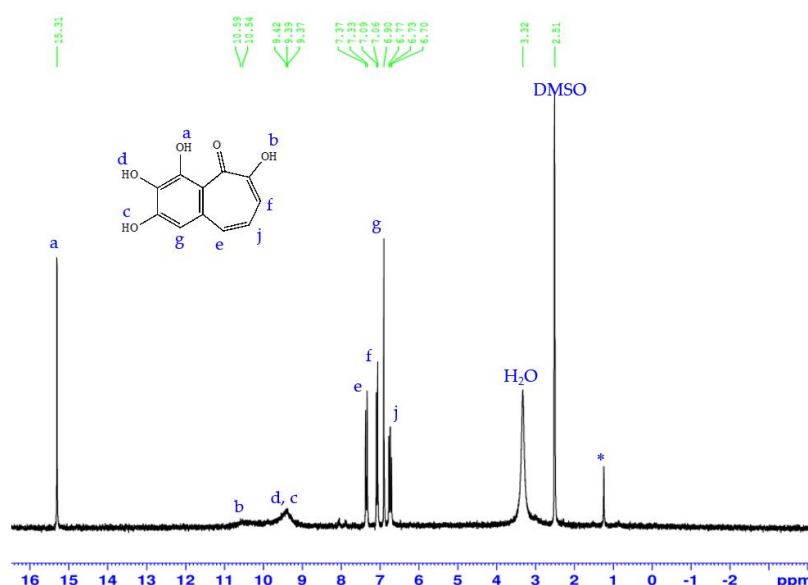


Figure 5. ¹H NMR spectrum of the product from HRP/GO_x@UiO-66-NH₂ catalysis. The presence of 2,3,4,6-tetrahydroxy-5H-benzocyclohept-5-one (also known as purpurogallin) confirms product formation in the solution from pyrogallol and glucose using the HRP/GO_x@UiO-66-NH₂ biocatalyst. * indicates hydrocarbon impurity.

2.6. Enzyme/MOF Immobilization and Leaching

Although both UiO-66 and UiO-66-NH₂ showed co-immobilization of both enzymes, UiO-66-NH₂ exhibited 6% greater enzyme immobilization than UiO-66, as shown in Table 2. This is likely due to enhanced electrostatic and H-bonding interactions imparted by the amine group attached to the organic linker in UiO-66-NH₂. Although maximum immobilization occurred with 24 hours of incubation, more data are required to signify immobilization percent yield. Nonetheless, the HRP/GO_x@UiO-66 composite material did show enhanced catalysis using the biocatalytic system, however, this composite lacks long-term stability in solution. Both enzymes have completely leached from UiO-66 by the end of the three-day leaching study, as shown in Table 2. Further investigation of the HRP/GO_x@UiO-66 stability showed that enzyme immobilization did not last over 24 hours in buffered solution. The discrepancy in solution stability between HRP/GO_x@UiO-66 and HRP/GO_x@UiO-66-NH₂ is likely due to weaker interactions at the enzyme/MOF interface as a result of differences in the surface of UiO-66 compared with UiO-66-NH₂. In Figure 6, the immobilization (a) and leaching (b) data demonstrate the enhanced stability from immobilization onto UiO-66-NH₂ in the HRP/GO_x@UiO-66-NH₂ composite. In addition to a higher percent immobilization (9.9%), the HRP/GO_x@UiO-66-NH₂ only loses 36% of enzyme loading after three days in buffered solution. Conversely, the HRP/GO_x@UiO-66 composite shows

lower enzyme loading (3.9% immobilization) and loses 100% of the adsorbed enzymes after only 24 hours in buffered solution. As shown in Table 2, the results for percent immobilization and composite stability correlate well with enzyme activity for the formation of purpurogallin, showing immobilization efficiency and indicating greater stability and enzyme loading increases enzyme activity. This study did not investigate individual enzyme loading. However, Lou et al. performed single immobilized soybean epoxide hydrolase (SEH) onto UiO-66-NH₂ to synthesize vicinal diols [13]. In the Lou et al. report, a shift in the N-H bending vibration of UiO-66-NH₂ was observed using XRD and FT-IR after immobilization with SEH via crosslinking. Lou et al. also reported high immobilization loading and solution stability for their SEH@UiO-66-NH₂ biocatalyst [13]; however, we are able to achieve comparable immobilization loading and composite stability using only surface adsorption to the MOF support. Based on our results for both UiO-66 and UiO-66-NH₂, as well as the results reported by Lou et al., it is apparent that MOF linker functionality plays a crucial role in maximizing loading and catalytic activity by enzyme immobilization on MOF supports.

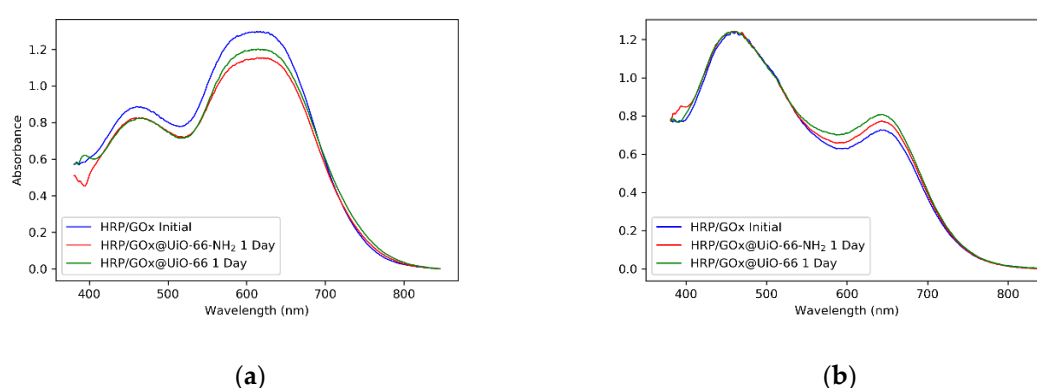


Figure 6. Immobilization and leaching in all composite materials. (a) UV/vis spectra of pure enzyme and enzyme/MOF solutions after 24 h showing a more dramatic decrease in absorbance at 595 nm for HRP/GO_x@UiO-66-NH₂ due to higher enzyme immobilization; (b) Leaching of enzymes to buffered solution from enzyme/MOF composites showing HRP/GO_x@UiO-66 leaching more enzyme to solution in comparison with HRP/GO_x@UiO-66-NH₂.

3. Materials and Methods

3.1. Materials

MOPSO buffer was prepared by diluting Bioworld 0.2 M MOPSO buffer with a pH of 6.5 to 50 mM buffered solution. Solid glucose oxidase from *Aspergillus niger* 145,200 U/g, solid β-D-Glucose, and solid pyrogallol were all purchased from Sigma Aldrich. Solid horseradish peroxidase 190 U/mL was purchased from Tokyo Chemical Industry (TCI). The reaction mixture of purpurogallin synthesis consisted of the following glucose to pyrogallol ratio in millimoles: 2:0.95 and 10 mg of enzyme/MOF composite, and 0.05 mg/mL of free enzyme solution for controls.

3.2. Methods

SEM images were collected on a JEOL JCM-7000 SEM. MOF suspensions were deposited on atomically flat silica wafers and were precoated using 10 nm Au nanoparticles to reduce charging. Using the immobilized 166:50 MOF-enzyme ratio of each composite, a working solution of 1 mg/mL of the composite material in methanol was prepared. After sonicating the working solution, 100 μL of it was further diluted in 8 mL of methanol. To prepare the disk sample, 11 μL of the diluted solution of each composite was dropped on the disk individually. Fourier-transform infrared attenuated total resonance spectroscopy (FT-IR-ATR) was used to characterize UiO-66 and UiO-66-NH₂ using a CARY 630 FT-IR Spectrometer. Zeta potentials of the MOFs—UiO-66 and UiO-66-NH₂—and the

enzyme/MOF composites—HRP/GO_x@UiO-66 and HRP/GO_x@UiO-66-NH₂—were measured using a Malvern Zetasizer Nano ZS. All solutions were prepped by dissolving 2 mg of MOF and 20 µL of total enzymes into 15 mL of 0.2 M MOPSO buffer with a pH of 6.5.

3.3. Synthesis of UiO-66 and UiO-66-NH₂

UiO-66 synthesis was completed as a one pot synthesis in a Teflon-lined reaction vessel based on a solvothermal synthesis reported by Shearer et al. [68]. Zirconium (IV) chloride (1.98 mmol) and terephthalic acid (1.98 mmol) precursors were dissolved in 34 mL DMF in the reaction vessel. An addition of 340 µL of concentrated hydrochloric acid moderator was then added to improve ligand solvent exchange. The solution was placed in a 120 °C oven and heated for 24 h. The resulting precipitate was washed 3 times with DMF, and once with methanol, before being collected by vacuum filtration. This process was repeated for the synthesis of UiO-66-NH₂ substituting 2-aminoterephthalic acid for terephthalic acid. Functional groups of the MOFs composites were identified using Fourier transform infrared attenuated total resonance (FT-IR-ATR) spectroscopy on a CARY 630 FT-IR spectrometer.

3.4. Enzyme Immobilization and Characterization

Enzymes were immobilized with MOFs in a MOPSO buffer system in an Erlenmeyer flask by shaking while incubating for 24 hours at cold temperatures maintained using gel ice packs. The following MOF to enzyme mass ratios (in mg) were utilized to study the immobilization capacity of both MOFs: 77:34, 166:50, and 30:45. All enzyme solutions consisted of 23% GO_x, 23% HRP, (both from 5 mg/mL stock enzyme solution) in 50 mM MOPSO buffer. In 10 mL of 50 mM MOPSO, pH 6.5 buffered solution, 5 mg of GO_x/HRP@MOF (at the mass ratios listed above) were shaken at room temperature for 3 days. Before and after incubation, the Bradford assay was performed on the centrifuged enzyme solution for spectrophotometric quantification using a Persee T8-DS Double Beam UV-Vis spectrometer to determine percent immobilization and percent leaching. The Bradford assay was carried out using Bio-rad Dye Protein Assay Dye Reagent Concentrate, and Bio-rad Lyophilized Bovine γ-Globin was used to form a standard concentration calibration curve.

4. Conclusions

The results of this investigation indicate that HRP/GO_x@UiO-66-NH₂ is the better biocatalyst for pyrogallol oxidation by activity and stability measurements. The enhanced catalytic activity observed in both enzyme/MOF systems studied show that enzyme immobilization onto metal-organic frameworks can increase reactivity for cooperative enzyme systems. The effect of linker functionalization on the enzyme/MOF interface also shows that the amine-functionalized MOF linker in HRP/GO_x@UiO-66-NH₂ enhances loading, reactivity, and stability when compared with HRP/GO_x@UiO-66. HRP/GO_x@UiO-66-NH₂ and HRP/GO_x@UiO-66 showed increased enzyme activity in comparison to free enzymes. The increase in enzyme loading and composite stability is likely due to the amine group increasing electrostatic attractive forces on the surface of the MOF for the enzymes used in this investigation. While the HRP/GO_x@UiO-66 also showed enhanced catalysis compared to free enzymes in the solution, it is not stable enough to maintain enzyme loading and catalytic enhancement over time.

Despite the low degree of spatial control, enzyme/MOF composite systems provide an adaptable, low cost material that can function effectively as a green biocatalyst for synthesis reactions, such as the one utilized in this investigation. The enzyme/MOF composite materials prepared in this study are both valid biocatalysts potentially useful for synthesizing organic compounds in different industries, such as pharmaceuticals. Schwartz and colleagues have shown a tradeoff between stability and activity when immobilizing enzymes by multipoint covalent attachment to a polymer [69]. While the enzymes in this study are not in multipoint covalent attachment, however, similar results were observed. After a month of storage, the measured absorbance at the λ_{\max} of the purpurogallin for HRP/GO_x@UiO-66-NH₂ composite decreased by 37%, while HRP/GO_x@UiO-66 decreased by 44%. This study demonstrates

that an analysis of structure and function relationships can be utilized to design better biocatalysts. Under investigation in our laboratory is determining the relationship between enzyme dynamics and its catalytic activity with the intent on preparing even more effective biocatalysts.

Author Contributions: Conceptualization, K.L.S. and D.S.K.; methodology, K.L.S. and D.S.K.; formal analysis, K.L.S. and D.S.K.; investigation, R.A., J.S. and S.R.; writing—original draft preparation, R.A.; writing—review and editing, R.A., K.L.S. and D.S.K.; supervision, K.L.S. and D.S.K.; project administration, K.L.S. and D.S.K.; All authors have read and agreed to the published version of the manuscript.

Funding: The APC was funded by Lewis University.

Acknowledgments: The authors would like to acknowledge the McCrone Group for the use of their SEM.

Conflicts of Interest: The authors declare no conflict of interest.

References

1. Zhou, H.-C. Enzyme–MOF (metal–organic framework) composites. *Royal Society of Chemistry* **2017**.
2. Rehm, B.H.A. Enzyme Engineering for in Situ Immobilization. *Molecules* **2016**, *21*. [[CrossRef](#)] [[PubMed](#)]
3. Shih, Y.H.; Lo, S.H.; Yang, N.S.; Singco, B.; Cheng, Y.J.; Wu, C.Y.; Chang, I.H.; Huang, H.Y.; Lin, C.H. Trypsin-Immobilized Metal–Organic Framework as a Biocatalyst in Proteomics Analysis. *ChemPlusChem* **2012**, *77*, 982–986. [[CrossRef](#)]
4. Ahmed, E.; Ismail, C.Z.D. Industrial Applications of Enzymes: Recent Advances, Techniques, and Outlooks. *Catalysts* **2018**, *8*, 238.
5. Rodrigues, R.C.; Ortiz, C.; Berenguer-Murcia, Á.; Torres, R.; Fernández-Lafuente, R. Modifying enzyme activity and selectivity by immobilization. *Chem. Soc. Rev.* **2013**, *42*, 6290–6307. [[CrossRef](#)]
6. Ki-Hyun Kim, A.D. Recent advances in enzyme immobilization techniques: Metal-organic frameworks as novel substrates. *Elev. Coord. Chem. Rev.* **2016**, *322*, 30–40.
7. Sheldon, R.A. Role of Biocatalysis in Sustainable Chemistry. *ACS Chem. Rev.* **2017**, *118*, 801–838. [[CrossRef](#)]
8. Gkaniatsou, E.; Sicard, C.; Ricoux, R.; Mahy, J.P.; Steunou, N.; Serre, C. Metal–organic frameworks: A novel host platform for enzymatic catalysis and detection. *Mater. Horizons* **2017**, *5*, 55–63. [[CrossRef](#)]
9. Ren, S.; Li, C.; Jiao, X.; Jia, S.; Jiang, Y.; Bilal, M.; Cui, J. Recent progress in multienzymes co-immobilization and multienzyme system applications. *Chem. Eng. J.* **2019**, *373*, 1254–1278. [[CrossRef](#)]
10. Homaei, A.A.; Sariri, R.; Vianello, F.; Stevanato, R. Enzyme immobilization: An update. *J. Chem. Biol.* **2013**, *6*, 185–205. [[CrossRef](#)]
11. Jesionowski, T.; Zdarta, J.; Krajewska, B. Enzyme immobilization by adsorption: A review. *Adsorption* **2014**, *20*, 801–821. [[CrossRef](#)]
12. Betancor, L.; Luckarift, H.R. Co-immobilized coupled enzyme systems in biotechnology. *Biotechnol. Genet. Eng. Rev.* **2013**, *27*, 95–114. [[CrossRef](#)] [[PubMed](#)]
13. Cao, S.L.; Yue, D.M.; Li, X.H.; Smith, T.J.; Li, N.; Zong, M.H.; Wu, H.; Ma, Y.Z.; Lou, W.Y. Novel Nano-/Micro-Biocatalyst: Soybean Epoxide Hydrolase Immobilized on UiO-66-NH₂ MOF for Efficient Biosynthesis of Enantiopure (R)-1, 2-Octanediol in Deep Eutectic Solvents. *ACS Sustain. Chem. Eng.* **2016**, *4*, 3586–3595. [[CrossRef](#)]
14. Shieh, F.K.; Wang, S.C.; Yen, C.I.; Wu, C.C.; Dutta, S.; Chou, L.Y.; Morabito, J.V.; Hu, P.; Hsu, M.H.; Wu, K.C.; et al. Imparting Functionality to Biocatalysts via Embedding Enzymes into Nanoporous Materials by a de Novo Approach: Size-Selective Sheltering of Catalase in Metal–Organic Framework Microcrystals. *J. Am. Chem. Soc.* **2015**, *137*, 4276–4279. [[CrossRef](#)] [[PubMed](#)]
15. Liu, W.L.; Yang, N.S.; Chen, Y.T.; Lirio, S.; Wu, C.Y.; Lin, C.H.; Huang, H.Y. Lipase-Supported Metal–Organic Framework Bioreactor Catalyzes Warfarin Synthesis. *Chem. Eur. J.* **2015**, *21*, 115–119. [[CrossRef](#)] [[PubMed](#)]
16. Fan, S.; Liang, B.; Xiao, X.; Bai, L.; Tang, X.; Lojou, E.; Cosnier, S.; Liu, A. Controllable Display of Sequential Enzymes on Yeast Surface with Enhanced Biocatalytic Activity toward Efficient Enzymatic Biofuel Cells. *J. Am. Chem. Soc.* **2020**, *4*, 3222–3230. [[CrossRef](#)] [[PubMed](#)]
17. Liu, W.L.; Wu, C.Y.; Chen, C.Y.; Singco, B.; Lin, C.H.; Huang, H.Y. Fast Multipoint Immobilized MOF Bioreactor. *Chem. Eur. J. Biocatal.* **2014**, *20*, 8923–8928. [[CrossRef](#)]
18. Jung, S.; Kim, Y.; Kim, S.J.; Kwon, T.H.; Huh, S.; Park, S. Bio-functionalization of metal–organic frameworks by covalent protein conjugation. *ChemComm* **2011**, *47*, 2904–2906. [[CrossRef](#)]

19. Zhou, H.-C. Coupling two enzymes into a tandem nanoreactor utilizing a hierarchically structured MOF. *RCS Chem. Sci.* **2016**, *7*. [[CrossRef](#)]
20. Patra, S.; Crespo, T.H.; Permyakova, A.; Sicard, C.; Serre, C.; Chaussé, A.; Steunou, N.; Legrand, L. Design of metal organic framework–enzyme based bioelectrodes as a novel and highly sensitive biosensing platform. *J. Mater. Chem. B* **2015**, *3*. [[CrossRef](#)]
21. Majewski, M.B.; Howarth, A.J.; Li, P.; Wasielewski, M.R.; Hupp, J.T.; Farha, O.K. Enzyme encapsulation in metal–organic frameworks for applications in catalysis. *RCS CrystEngComm* **2017**. [[CrossRef](#)]
22. Distefano, M.D. Site-Specific, Covalent Attachment of Proteins to a Solid Surface. *Bioconjugate Chem.* **2006**, *17*, 967–974. [[CrossRef](#)]
23. Morten Meldal, S.S. Recent advances in covalent, site-specific protein immobilization. *F1000Research* **2016**, *5*, 1–11.
24. Wang, X.; Lu, X.; Wu, L.; Chen, J. 3D metal-organic framework as highly efficient biosensing platform for ultrasensitive and rapid detection of bisphenol A. *Biosens. Bioelectron.* **2015**, *65*, 295–301. [[CrossRef](#)] [[PubMed](#)]
25. Ashlee, J.; Howarth, Y.L. Chemical, thermal and mechanical stabilities of metal–organic frameworks. *Nat. Rev. Mater.* **2016**. [[CrossRef](#)]
26. Liang, K. Biomimetic mineralization of metal-organic frameworks as protective coatings for biomacromolecules. *Nat. Commun.* **2015**, *6*. [[CrossRef](#)] [[PubMed](#)]
27. Patterson, J.P. Direct Observation of Amorphous Precursor Phases in the Nucleation of Protein–Metal–Organic Frameworks. *J. Am. Chem. Soc.* **2020**, 1433–1442. [[CrossRef](#)]
28. Kenneth, J.; Balkus, J. Hybrid materials for immobilization of MP-11 catalyst. *Top. Catal.* **2006**, *36*. [[CrossRef](#)]
29. Feng, D.; Liu, T.F.; Su, J.; Bosch, M.; Wei, Z.; Wan, W.; Yuan, D.; Chen, Y.P.; Wang, X.; Wang, K.; et al. Stable metal-organic frameworks containing single-molecule traps for enzyme encapsulation. *Nat. Commun.* **2015**, *6*. [[CrossRef](#)]
30. Zhu, L.; Yang, R.; Zhai, J.; Tian, C. Bienzymatic glucose biosensor based on co-immobilization of peroxidase and glucose oxidase on a carbon nanotubes electrode. *Biosens. Bioelectron.* **2007**, *23*, 528–535. [[CrossRef](#)]
31. Garcia-Galan, C.; Berenguer-Murcia, Á.; Fernandez-Lafuente, R.; Rodrigues, R.C. Potential of Different Enzyme Immobilization Strategies to Improve Enzyme Performance. *Adv. Synth. Catal.* **2011**, *353*, 2885–2904. [[CrossRef](#)]
32. Pitzalis, F.; Monduzzi, M.; Salis, A. A bienzymatic biocatalyst constituted by glucose oxidase and Horseradish peroxidase immobilized on ordered mesoporous silica. *Microporous Mesoporous Mater.* **2017**, *241*, 145–154. [[CrossRef](#)]
33. Barbosa, O.; Torres, R.; Ortiz, C.; Berenguer-Murcia, A.; Rodrigues, R.C.; Fernandez-Lafuente, R. Rodrigues, Roberto Fernandez-Lafuente. Heterofunctional Supports in Enzyme Immobilization: From Traditional Immobilization Protocols to Opportunities in Tuning Enzyme Properties. *Biomacromolecules* **2013**, *8*, 2433–2462. [[CrossRef](#)] [[PubMed](#)]
34. Don, A.; Cowana, R.F.-L. Enhancing the functional properties of thermophilic enzymes by chemical modification and immobilization. *Enzyme Microb. Technol.* **2011**, *49*, 326–346.
35. Rios, N.S.; Arana-Peña, S.; Mendez-Sanchez, C.; Ortiz, C.; Gonçalves, L.R.; Fernandez-Lafuente, R. Gonçalves, and Roberto Fernandez-Lafuente Reuse of Lipase from *Pseudomonas fluorescens* via Its Step-by-Step Coimmobilization on Glyoxyl-Octyl Agarose Beads with Least Stable Lipases. *Catalysts* **2019**, *9*, 487. [[CrossRef](#)]
36. Marshall, R.J.; Forgan, R.S. Postsynthetic Modification of Zirconium Metal-Organic Frameworks. *Eur. J. Inorg. Chem.* **2016**, 4310–4331. [[CrossRef](#)]
37. Smith, M.R.; Gao, H.; Prabhu, P.; Bugada, L.F.; Roth, C.; Mutukuri, D.; Yee, C.M.; Lee, L.; Ziff, R.M.; Lee, J.K.; et al. Elucidating structure–performance relationships in whole-cell cooperative enzyme catalysis. *Nat. Catal.* **2019**, *2*, 809–819. [[CrossRef](#)]
38. Bugada, L.F.; Smith, M.R.; Wen, F. Engineering Spatially Organized Multienzyme Assemblies for Complex Chemical Transformation. *ACS Catal.* **2018**, *8*, 7898–7906. [[CrossRef](#)]
39. Ananthanarayan, L. Glucose oxidase—An overview. *Biotechnol. Adv.* **2009**, *27*, 489–501. [[CrossRef](#)]
40. Veitch, N.C. Horseradish peroxidase: A modern view of a classic enzyme. *Phytochemistry* **2004**, *65*, 249–259. [[CrossRef](#)]
41. Gao, F.; Guo, Y.; Fan, X.; Hu, M.; Li, S.; Zhai, Q.; Jiang, Y.; Wang, X. Enhancing the catalytic performance of chloroperoxidase by coimmobilization with glucose oxidase on magnetic graphene oxide. *Biochem. Eng. J.* **2018**, *143*, 101–109. [[CrossRef](#)]

42. Liu, Y. Hemin@metal–organic framework with peroxidaselike activity and its application to glucose detection. *RCS Catal. Sci. Technol.* **2013**, *3*, 2761–2768. [[CrossRef](#)]
43. Jia, F.; Zhang, Y.; Narasimhan, B.; Mallapragada, S.K. Block Copolymer-Quantum Dot Micelles for Multienzyme Colocalization. *ACS Langmuir* **2012**, *28*, 17389–17395. [[CrossRef](#)]
44. Gustafsson, H.; Küchler, A.; Holmberg, K.; Walde, P. Co-immobilization of enzymes with the help of a dendronized polymer and mesoporous silica nanoparticles. *RCS Mater. Chem. B* **2012**, 1–3. [[CrossRef](#)] [[PubMed](#)]
45. Yang, K.L. Combined cross-linked enzyme aggregates of horseradish peroxidase and glucose oxidase for catalyzing cascade chemical reactions. *Enzyme Microbial Technol.* **2017**, *100*, 52–59. [[CrossRef](#)]
46. Memon, A.H.; Ding, R.; Yuan, Q.; Liang, H.; Wei, Y. Coordination of GMP ligand with Cu to enhance the multiple enzymes stability and substrate specificity by co-immobilization process. *Biochem. Eng. J.* **2018**, *136*, 102–108. [[CrossRef](#)]
47. Wu, X.; Yang, C.; Ge, J. Green synthesis of enzyme/ metal-organic framework composites with high stability in protein denaturing solvents. *Bioresour. Bioprocess.* **2017**, *4*. [[CrossRef](#)]
48. Chen, S.; Wen, L.; Svec, F.; Tan, T.; Lv, Y. Magnetic metal–organic frameworks as scaffolds for spatial co-location and positional assembly of multi-enzyme systems enabling enhanced cascade biocatalysis. *RCS Adv.* **2017**, *7*, 21205–21213. [[CrossRef](#)]
49. Vriezema, D.M.; Garcia, P.M.; Sancho Oltra, N.; Hatzakis, N.S.; Kuiper, S.M.; Nolte, R.J.; Rowan, A.E.; van Hest, J.C. Positional Assembly of Enzymes in Polymersome Nanoreactors for Cascade Reactions. *Angew. Chem. Commun. Nanoreactors* **2007**, *46*, 7378–7382. [[CrossRef](#)]
50. Kazenwadel, F. Synthetic enzyme supercomplexes: Coimmobilization of enzyme cascades. *RSC Anal. Methods* **2015**, *7*, 4030–4037. [[CrossRef](#)]
51. van de Velde, F.; Lourenço, N.D.; Bakker, M.; van Rantwijk, F.; Sheldon, R.A. Sheldon. Improved Operational Stability of Peroxidases by Coimmobilization with Glucose Oxidase. *Biotechnol. Bioeng.* **2000**, *69*, 286–291. [[CrossRef](#)]
52. Jia, F.; Narasimhan, B.; Mallapragada, S.K. Biomimetic Multienzyme Complexes Based on Nanoscale Platforms. *AIChE* **2012**, *59*. [[CrossRef](#)]
53. Li, Z.; Zhang, Y.; Su, Y.; Ouyang, P.; Ge, J.; Liu, Z. Spatial co-localization of multi-enzymes by inorganic nanocrystal–protein complexes. *RCS ChemComm* **2014**, *50*, 12465–12468. [[CrossRef](#)] [[PubMed](#)]
54. Müller, J.; Niemeyer, C.M. DNA-directed assembly of artificial multienzyme complexes. *Biochem. Biophys. Res. Commun.* **2008**, *377*, 62–67. [[CrossRef](#)]
55. Park, H.Y. Purpurogallin exerts anti-inflammatory effects in lipopolysaccharide-stimulated BV2 microglial cells through the inactivation of the NF- κ B and MAPK signaling pathways. *Int. J. Mol. Med.* **2013**, *32*, 1171–1178. [[CrossRef](#)]
56. Bilal, M.; Mehmood, S.; Rasheed, T.; Iqbal, H. Bio-Catalysis and Biomedical Perspectives of Magnetic Nanoparticles as Versatile Carriers. *Magnetochemistry* **2019**, *5*. [[CrossRef](#)]
57. Bosio, V.E.; Islan, G.A.; Martínez, Y.N.; Durán, N.; Castro, G.R. Nanodevices for the immobilization of therapeutic enzymes. *Crit. Rev. Biotechnol.* **2016**, *36*, 447–464. [[CrossRef](#)]
58. Wang, W.; Wang, L.; Li, Y.; Liu, S.; Xie, Z.; Jing, X. Nanoscale Polymer Metal–Organic Framework Hybrids for Effective Photothermal Therapy of Colon Cancers. *Adv. Mater.* **2016**, *28*, 9320–9325. [[CrossRef](#)]
59. Ramasarma, T. New insights of superoxide dismutase inhibition of pyrogallol autoxidation. *Mol. Cell. Biochem.* **2014**, *400*, 277–285. [[CrossRef](#)]
60. Fernandez, M.; Frydman, R.B.; Hurst, J.; Buldain, G. Structure/activity relationships in porphobilinogen oxygenase and horseradish peroxidase an analysis using synthetic hemins. *Eur. J. Biochem.* **1993**, *218*, 251–259. [[CrossRef](#)]
61. Bradford, M.M. A rapid and sensitive method for the quantitation of microgram quantities of protein utilizing the principle of protein–dye binding. *Elsevier Anal. Biochem.* **1976**, *72*, 248–254. [[CrossRef](#)]
62. Salopek, B.; Krasic, D.; Filipovic, S. Measurement and application of zeta-potential. *Rudarsko-geolosko-Naftni Zbornik* **1992**, *4*, 147–151.
63. Guo, X. Facile synthesis of morphology- and size-controlled zirconium metal-organic framework UiO-66: The role of hydrofluoric acid in crystallization. *CrystEngComm* **2015**, *17*, 6434–6440. [[CrossRef](#)]
64. Wu, L. Electronic effects of ligand substitution on metal–organic framework photocatalysts: The case study of UiO-66. *PCCP* **2015**, *17*, 117–121. [[CrossRef](#)]

65. Wang, S. Amino-functionalized Zr-MOF nanoparticles for adsorption of CO₂ and CH₄. *Int. J. Smart Nano Mater.* **2013**, *4*, 72–82. [[CrossRef](#)]
66. Zhou, J.J.; Wang, R.; Liu, X.L.; Peng, F.M.; Li, C.H.; Teng, F.; Yuan, Y.P. In situ growth of CdS nanoparticles on UiO-66 metal-organic framework octahedrons for enhanced photocatalytic hydrogen production under visible light irradiation. *Appl. Surf. Sci.* **2015**, *346*, 278–283. [[CrossRef](#)]
67. Boudrant, J.; Woodley, J.M.; Fernandez-Lafuente, R. Parameters necessary to define an immobilized enzyme preparation. *Process Biochem.* **2019**, *90*, 66–80. [[CrossRef](#)]
68. Lillerud, K.P. Tuned to Perfection: Ironing out the Defects in Metal-Organic Framework UiO-66. *Chem. Mater.* **2016**, *14*, 4068–4071. [[CrossRef](#)]
69. Weltz, J.S.; Kienle, D.F.; Schwartz, D.K.; Kaar, J.L. Reduced Enzyme Dynamics upon Multipoint Covalent Immobilization Leads to Stability-Activity Trade-off. *J. Am. Chem. Soc.* **2020**, *142*, 3463–3471. [[CrossRef](#)]



© 2020 by the authors. Licensee MDPI, Basel, Switzerland. This article is an open access article distributed under the terms and conditions of the Creative Commons Attribution (CC BY) license (<http://creativecommons.org/licenses/by/4.0/>).